Steel and Composite Structures, *Vol. 35, No. 1* (*2020*) *43-59*
DOI: https://doi.org/10.12989/scs.2020.35.1.043

Finite element vibration analysis of laminated composite parabolic thick plate frames

Oguzhan Das*[1], Hasan Ozturk[2a] and Can Gonenli[1b]

[1]*The Graduate School of Natural and Applied Sciences, Dokuz Eylul University, Tinaztepe Campus, Buca – İzmir, 35390 Turkey*
[2]*Department of Mechanical Engineering, Dokuz Eylul University, Tinaztepe Campus, Buca – İzmir, 35390 Turkey*

(*Received June 10, 2019, Revised February 9, 2020, Accepted February 13, 2020*)

Abstract. In this study, free vibration analysis of laminated composite parabolic thick plate frames by using finite element method is introduced. Governing equations of an eigenvalue problem are obtained from First Order Shear Deformation Theory (FSDT). Finite element method is employed to obtain natural frequency values from the governing differential equations. The frames consist of two flat square plates and one singly curved plate. Parameters like radii of curvature, aspect ratio, ply orientation and boundary conditions are investigated to understand their effect on dynamic behavior of such a structure. In addition, multi-bay structures of such geometry with different stacking order are also taken into account. The composite frame structures are also modeled and simulated via ANSYS to verify the accuracy of the present study.

Keywords: vibration analysis; parabolic frames; composite structures; first order shear deformation theory; finite element analysis

1. Introduction

Plate frame structures are utilized in various applications of engineering, like the marine industry, aircraft, and many other structures. Advancements in composite materials, on the other hand, enables to lighten and strengthen these structures. Mechanical properties of such a structure can be varied by changing lamination material, lamination angle, stacking sequence. Although numerous studies about laminated composite frame structures are reported in the literature, it has been seen that there has not been any published paper about laminated composite parabolic thick plate frames. There are several similar studies about composite folded plates (Wittrick and Horsington 1984, Liu and Huang 1992, Peng 2015), which are dealt with flat folded plates with different methods and theories.

Vibration analysis of structures like beams, plates, frames, etc. has been a popular field of interest for a long time. Since mentioning about all studies is not possible, some publications are discussed as follows briefly. Marbur and Kant (1996) carried out a study that was aimed to conduct free vibration analysis of fiber-reinforced composite beams by utilizing the Higher-Order Shear Deformation Theory (HSDT). They also investigated the dynamical behavior of sandwich composite beams in that work. Atlihan *et al.* (2009) utilized the Differential Quadrature Method (DQM) to perform free vibration analysis of a laminated composite beam. Ramtekkar (2009) used a 2-D plane stress mixed finite element model in order to perform a free vibration analysis of laminated beams with delaminations. Jun and Hongxing (1996) investigated the free vibration behavior of axially loaded laminated composite beams by using Higher Order Shear Deformation Theory. They introduced the dynamic stiffness matrix method to solve both free vibration and buckling problems. In addition, several boundary conditions. Ozturk (2012) investigated the vibration analysis of a pre-stress laminated composite curved beam. In that study, a curved beam was modeled by utilizing the Finite Element Method with a straight beam element. In addition, to obtain the curved shape, the Reversion Method was used to obtain a non-linear deflection curve. Narita and Leissa (1992) presented an analytical approach to investigate the free vibration of cantilevered and symmetrically laminated rectangular plates by using the Ritz method. Afshari and Widera (2000) developed a series of the plate by considering the modified complementary energy principle formulations for free vibration analysis of composite plates. Pandit *et al.* (2007) investigated the free vibration analysis of composite rectangular plates by using a nine node isoparametric bending element with an effective mass lumping scheme. Besides simple rectangular plates, they also obtained natural frequency results not only for plates that have cutouts but also for plates on which distributed mass exists. Ngo-Cong *et al*. (2011) presented an effective Radial Basis Function for free vibration analysis of laminated composite plates via

∗Corresponding author, Ph.D. Candidate
E-mail: oguzhan.das@deu.edu.tr
[a]Professor
E-mail: hasan.ozturk@deu.edu.tr
[b]Ph.D. Candidate
E-mail: can.gonenli@deu.edu.tr

ISSN: 1229-9367 (Print), 1598-6233 (Online)

the First-Order Shear Deformation Theory (FSDT). Ganesh et al. (2016) studied the free vibration analysis of laminated composite plates by using the finite element method and by considering several boundary conditions. Helloty (2016) examined parameters that affect the free vibration analysis of stiffened laminated composite plates. Belarbi *et al*. (2017) developed a higher-order layerwise finite element model for the free vibration analysis of multilayer sandwich plates. Fallah and Delzendeh (2018) utilized a Meshless Finite Volume (MFV) method for free vibration analysis of laminated composite plates. They tested MFV for different parameters such as plate thickness, stacking sequences, boundary conditions, and plate shapes. Cantin and Glough (1968) developed a curved cylindrical shell finite element for curved shells and proceeded a finite element analysis to find the displacement of a curved shell. Petyt and Deb Nath (1971) conducted a free vibration analysis for singly curved rectangular plates. Yas and Chakravorty *et al.* (1996) presented a finite element analysis for free vibration analysis of doubly curved shells by using First-Order Shear Deformation Theory. Garmsiri (2010) investigated three-dimensional free vibration analysis of fiber-reinforced functionally graded cylindrical shells by using differential quadrature method (DQM). Ye *et al.* (2013) studied on free vibration analysis of laminated composite shallow shells with general elastic boundaries by using Rayleigh–Ritz procedure. Javed *et al.* (2016) studied on free vibration analysis of composite shells that have non-uniform thickness walls by using first-order shear deformation theory. Javed *et al*. (2016) utilized higher-order shear deformation theory to perform vibration analysis of antisymmetric angle-ply laminated plates for simply supported boundary conditions. Civalek (2017) investigated the vibration behavior of laminated composite truncated conical panels and annular sector panels with functionally graded materials (FGM) by using Love's shell theory and First Order Shear Deformation Theory. Governing differential equations of this study were solved via Differential Quadrature (DQ) and Discrete Singular Convolution (DSC) method. Chaubey and Kumar (2017) conducted a free vibration finite element analysis of laminated composite cylindrical, spherical, hypar, saddle, and elliptical shells with cutouts and concentrated mass by using Third Order Shear Deformation Theory (TSDT). Javed *et al*. (2018) used higher-order shear deformation theory to evaluate the natural frequency values of the cross-ply laminated plates depending on the aspect ratio, side-to-thickness ratio, number of laminae, ply orientations, and stacking sequence. Hafizah and Viswanathan (2018) studied on the vibration of antisymmetric angle-ply composite annular plates by using first-order shear deformation theory and considering linear, exponential, and sinusoidal thickness variations. Guha Niyogi *et al.* (1993) modeled laminated composite folded structures and performed free and forced finite element vibration analysis by using First-Order Shear Deformation Theory. Haldar and Sheikh (2005) presented a flexible shear element to conduct free vibration analysis of both isotropic and laminated composite plates. Thinh *et al*. (2012) studied finite element bending and vibration analysis of multi-folding laminated composite plates by using First-Order Shear Deformation Theory.

This paper presents the free vibration finite element analysis of laminated parabolic thick plate frames (LCPTPF), which includes two square flat plates and one singly curved plate which is perpendicular to those flat plates. Governing equations are obtained by using First-Order Shear Deformation Theory (FSDT). In order to perform finite element analysis, 4-node quadrilateral plate element and similarly, 4-node cylindrical shell element is utilized. Although both elements are used widely, it has been seen that there has not been any study about the combination of those elements in order to model a frame structure. This study proves that these two elements are in good agreement when integrated with each other. The natural frequency results of free vibration analysis of LCPTPF are obtained for several parameters such as curvature, aspect ratio, boundary conditions, stacking orders, and multi-bay structure. For comparison, the same structure is modeled and simulated via ANSYS. It is seen that finite element analysis results show good agreement with simulation results.

2. Mathematical formulation

In order to proceed free vibration analysis of LCPTPF, which is shown in Fig. 1, it is necessary to select an appropriate finite element and plate theory for both flat and curved plates. For flat plates, the four-node quadrilateral plate element that is shown in Fig. 2 is used. For the curved plate, on the other hand, the four-node cylindrical shell element, which is shown in Fig. 3, is utilized. The First Order Shear Deformation (FSDT) theory is selected as the plate theory for free vibration analysis of LCPTPF.

Although there are numerous methods for analyzing composite structures, First Order Shear Deformation Theory (FSDT), an equivalent single-layer theory, is utilized to perform finite element free vibration analysis of LCPTPF. For an orthotropic laminated composite plate with n-layers, which is shown in Fig. 4, displacement components can be written as in Eq. (1).

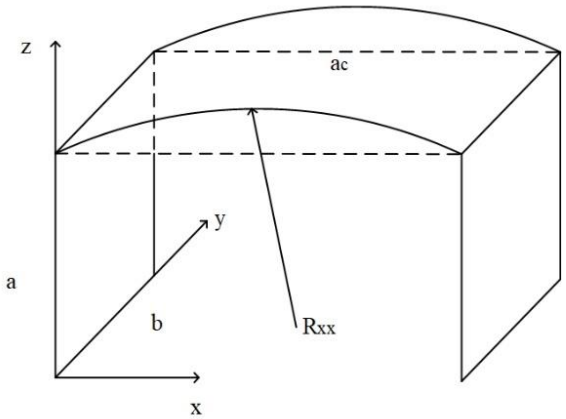

Fig. 1 Laminated Parabolic Thick Plate Frame

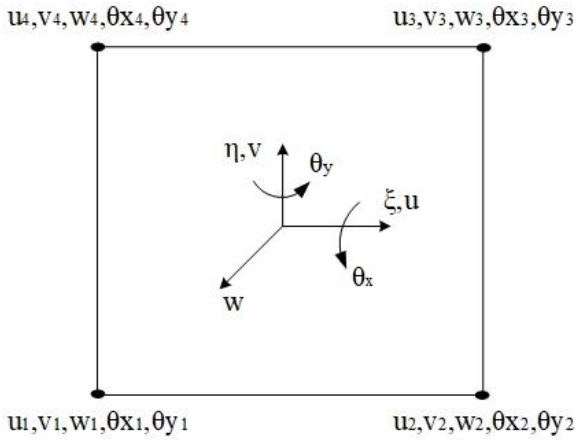

Fig. 2 Four-node quadrilateral element

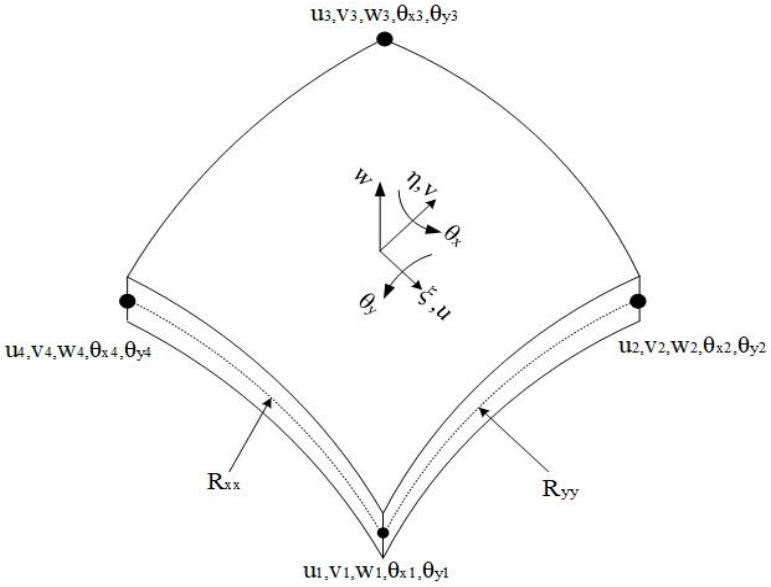

Fig. 3 Four-node cylindrical shell element

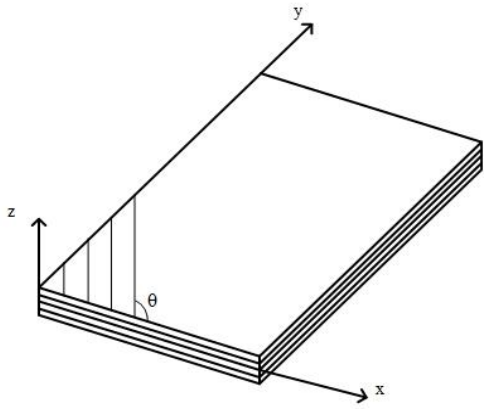

Fig. 4 Laminated Composite Plate

$$u(x,y,z) = u_0(x,y) + z\theta_y(x,y)$$
$$v(x,y,z) = v_0(x,y) + z\theta_x(x,y) \quad (1)$$
$$w(x,y,z) = w_0(x,y)$$

Strain relations in accordance with displacements can be written as

$$\varepsilon_{xx} = \frac{\partial u}{\partial x} = \frac{\partial u_0}{\partial x} - z\frac{\partial \theta_y}{\partial x}$$
$$\varepsilon_{yy} = \frac{\partial v}{\partial y} = \frac{\partial v_0}{\partial y} + z\frac{\partial \theta_x}{\partial y}$$
$$\gamma_{xy} = \frac{\partial u}{\partial y} + \frac{\partial v}{\partial x} = \frac{\partial v_0}{\partial x} + \frac{\partial u_0}{\partial y} + z\left(\frac{\partial \theta_x}{\partial x} - \frac{\partial \theta_y}{\partial y}\right) \quad (2)$$
$$\gamma_{xz} = -\theta_y + \frac{\partial w}{\partial x}$$
$$\gamma_{yz} = \theta_x + \frac{\partial w}{\partial y}$$

or

$$\{\varepsilon\} = \{\varepsilon_0\} - \{\varepsilon_1\} = \begin{bmatrix} \frac{\partial u_0}{\partial x} \\ \frac{\partial v_0}{\partial y} \\ \frac{\partial v_0}{\partial x} + \frac{\partial u_0}{\partial y} \end{bmatrix} + z\begin{bmatrix} -\frac{\partial \theta_y}{\partial x} \\ \frac{\partial \theta_x}{\partial y} \\ \frac{\partial \theta_x}{\partial x} - \frac{\partial \theta_y}{\partial y} \end{bmatrix} \quad (3)$$
$$\{\gamma_0\} = \begin{bmatrix} -\theta_y + \frac{\partial w}{\partial x} \\ \theta_x + \frac{\partial w}{\partial y} \end{bmatrix}$$

In order to perform finite element analysis, a four-node quadrilateral plate element with five degrees of freedom at each node is considered. Displacement representation for each node is given as

$$u = \sum_{i=1}^{4} u_i N_i \qquad v = \sum_{i=1}^{4} v_i N_i \qquad w = \sum_{i=1}^{4} w_i N_i$$
$$\theta_y = \sum_{i=1}^{4} \theta_{yi} N_i \qquad \theta_x = \sum_{i=1}^{4} \theta_{xi} N_i \quad (4)$$

Substituting Eq. (3) into Eq. (2) and writing in matrix form gives the strain matrix, which can be defined as

$$[\boldsymbol{B_s}] = \begin{bmatrix} \varepsilon_{xx} \\ \varepsilon_{yy} \\ \gamma_{xy} \\ \gamma_{xz} \\ \gamma_{yz} \end{bmatrix} = \sum_{i=1}^{4} \begin{bmatrix} \frac{\partial N_i}{\partial x} & 0 & 0 & 0 & 0 \\ 0 & \frac{\partial N_i}{\partial y} & 0 & 0 & 0 \\ \frac{\partial N_i}{\partial y} & \frac{\partial N_i}{\partial x} & 0 & 0 & 0 \\ 0 & 0 & 0 & 0 & -\frac{\partial N_i}{\partial x} \\ 0 & 0 & 0 & \frac{\partial N_i}{\partial y} & 0 \\ 0 & 0 & 0 & \frac{\partial N_i}{\partial x} & -\frac{\partial N_i}{\partial y} \\ 0 & 0 & \frac{\partial N_i}{\partial x} & 0 & -N_i \\ 0 & 0 & \frac{\partial N_i}{\partial y} & N_i & 0 \end{bmatrix} \begin{bmatrix} u_i \\ v_i \\ w_i \\ \theta_{xi} \\ \theta_{yi} \end{bmatrix} \quad (5)$$

The constitutive relations of a layer of a laminated plate can be written with respect to the fiber-matrix axis as

$$\begin{bmatrix} \sigma_1 \\ \sigma_2 \\ \tau_{12} \\ \tau_{13} \\ \tau_{23} \end{bmatrix} = \begin{bmatrix} q_{11} & q_{12} & 0 & 0 & 0 \\ q_{12} & q_{22} & 0 & 0 & 0 \\ 0 & 0 & q_{66} & 0 & 0 \\ 0 & 0 & 0 & q_{44} & 0 \\ 0 & 0 & 0 & 0 & q_{55} \end{bmatrix} \begin{bmatrix} \varepsilon_1 \\ \varepsilon_2 \\ \gamma_{12} \\ \gamma_{13} \\ \gamma_{14} \end{bmatrix} \quad (6)$$

where

$$q_{11} = \frac{E_1}{1 - \vartheta_{12}\vartheta_{21}}$$
$$q_{12} = \frac{\vartheta_{12}E_2}{1 - \vartheta_{12}\vartheta_{21}}$$
$$q_{22} = \frac{E_2}{1 - \vartheta_{12}\vartheta_{21}}$$
$$q_{66} = G_{12}$$
$$q_{44} = G_{13} \quad (7)$$
$$q_{55} = G_{23}$$
$$E_1\vartheta_{21} = E_2\vartheta_{12}$$

Since the stress and strain relations are given in local coordinates (along fibers), it is needed to transform these relations into the global coordinate axis *(x,y,z)*. The stress and strain relations of the kth lamina in global axis can be expressed as

$$[\boldsymbol{\sigma}]^k = [\boldsymbol{Q}]^k\{\varepsilon\} \quad (8)$$

or

$$\begin{bmatrix} \sigma_{xx} \\ \sigma_{yy} \\ \tau_{xy} \\ \tau_{xz} \\ \tau_{yz} \end{bmatrix}^k = \begin{bmatrix} Q_{11} & Q_{12} & Q_{16} & 0 & 0 \\ Q_{12} & Q_{22} & Q_{26} & 0 & 0 \\ Q_{16} & Q_{26} & Q_{66} & 0 & 0 \\ 0 & 0 & 0 & Q_{44} & 0 \\ 0 & 0 & 0 & 0 & Q_{55} \end{bmatrix}^k \begin{bmatrix} \varepsilon_{xx} \\ \varepsilon_{yy} \\ \gamma_{xy} \\ \gamma_{xz} \\ \gamma_{yz} \end{bmatrix} \quad (9)$$

where

$$\mathrm{Q}_{11} = q_{11}c^4 + 2(q_{12} + 2q_{66})s^2c^2 + q_{22}s^4$$
$$\mathrm{Q}_{12} = (q_{11} + \ q_{22} - 4q_{66})s^2c^2 + q_{12}(s^4 + c^4)$$
$$\mathrm{Q}_{22} = q_{11}s^4 + 2(q_{12} + 2q_{66})s^2c^2 + q_{22}c^4$$
$$\mathrm{Q}_{16} = (q_{11} - \ q_{12} - 2q_{66})sc^3 + (q_{12} - \ q_{22} + 2q_{66})s^3c$$
$$\mathrm{Q}_{26} = (q_{11} - \ q_{12} - 2q_{66})s^3c + (q_{12} - \ q_{22} + 2q_{66})sc^3 \quad (10)$$
$$\mathrm{Q}_{66} = (q_{11} + \ q_{22} - 2q_{12} - 2q_{66})s^2c^2 + q_{66}(s^4 + c^4)$$
$$Q_{44} = q_{55}s^2 + q_{44}c^2$$
$$Q_{45} = q_{55}cs - q_{44}cs$$
$$Q_{55} = q_{55}c^2 + q_{44}s^2$$

where c and s denote cosθ, and sinθ, respectively. θ is the fiber angle. The strain energy stored in a structure can be expressed as

$$U = \frac{1}{2}\int_V \sigma\varepsilon dv \quad (11)$$

If Eqs. (4)-(8) are substituted into Eq. (10), the strain energy equation for laminated plates become as

$$U = \frac{1}{2}\int_A (\{\varepsilon_0\}^T[\boldsymbol{A}]\{\varepsilon_0\} - \{\varepsilon_0\}^T[\boldsymbol{B}]\{\varepsilon_1\} - \{\varepsilon_1\}^T[\boldsymbol{B}]\{\varepsilon_0\} + \{\varepsilon_1\}^T[\boldsymbol{C}]\{\varepsilon_1\})\,dA + \frac{1}{2}\int_A p^*\{\gamma_0\}^T[\boldsymbol{As}]\{\gamma_0\} \quad (12)$$

where $\mathbf{[A]}_{3x3}$, $\mathbf{[B]}_{3x3}$, $\mathbf{[C]}_{3x3}$, and $\mathbf{[A_s]}_{2x2}$, which are given in Eq. (13) represents longitudinal, bending-longitudinal coupled, bending and shear effects respectively.

According to FSDT, shear stress is constant through thickness. However, it is known that in three-dimensional analysis, such variation should be at least quadratic. In order to satisfy that, a shear correction factor *(p*)* is introduced. While there is a method to calculate that factor, it is generally taken as 5/6 or π2/12.

$$[\boldsymbol{A}] = \sum_{k=1}^{NL}[\boldsymbol{Q_{bm}}]^k(z_{k+1} - z_k)$$
$$[\boldsymbol{B}] = \frac{1}{2}\sum_{k=1}^{NL}[\boldsymbol{Q_{bm}}]^k(z_{k+1}^2 - z_k^2)$$
$$[\boldsymbol{C}] = \frac{1}{3}\sum_{k=1}^{NL}[\boldsymbol{Q_{bm}}]^k(z_{k+1}^3 - z_k^3) \quad (13)$$
$$[\boldsymbol{A_s}] = \sum_{k=1}^{NL}[\boldsymbol{Q_s}]^k(z_{k+1} - z_k)$$

where z_k is the kth layer of laminated plate and *NL* is the number of layers. $[\boldsymbol{Q_{bm}}]$ and $[\boldsymbol{Q_s}]$ are

$$[\boldsymbol{Q_{bm}}]^k = \begin{bmatrix} Q_{11} & Q_{12} & Q_{16} \\ Q_{12} & Q_{22} & Q_{26} \\ Q_{16} & Q_{26} & Q_{66} \end{bmatrix}^k \quad (14)$$
$$[\boldsymbol{Q_s}]^k = \begin{bmatrix} Q_{44} & 0 \\ 0 & Q_{55} \end{bmatrix}^k$$

The element stiffness matrix is obtained by using strain energy equation as

$$[\boldsymbol{k_e}] = \frac{1}{2}\int_A [\boldsymbol{B_s}]^{\boldsymbol{T}}[\boldsymbol{D}][\boldsymbol{B_s}]\boldsymbol{dA} \quad (15)$$

where

$$[\boldsymbol{D}] = \begin{bmatrix} [\boldsymbol{A}] & [\boldsymbol{B}] & 0 \\ [\boldsymbol{B}] & [\boldsymbol{C}] & 0 \\ 0 & 0 & p^*[\boldsymbol{As}] \end{bmatrix} \quad (16)$$

The kinetic energy equation can be written as

$$T = \frac{1}{2}\int_A \rho^k(u^2 + v^2 + w^2)dA \quad (17)$$

Substituting Eq. (1) into Eq. (17) gives

$$T = \frac{1}{2}\int_A (I\dot{u_0}^2 + I\dot{v_0}^2 + I\dot{w_0}^2 + P\dot{\theta}_y^2 + P\dot{\theta}_x^2 + V\dot{\theta}_y^2 + V\dot{\theta}_x^2)dA \quad (18)$$

where

$$I = \rho\int_{-h/2}^{h/2} dz$$
$$P = \rho\int_{-h/2}^{h/2} z\,dz \quad (19)$$
$$V = \rho\int_{-h/2}^{h/2} z^2\,dz$$

The element mass matrix can be obtained from the kinetic energy equation as

$$[\boldsymbol{m_e}] = \frac{1}{2}\int_A [\boldsymbol{N}]^T[\boldsymbol{IPQ}][\boldsymbol{N}]\,dA \quad (20)$$

where **[N]** is the shape function matrix for each node which is given as

$$[\boldsymbol{N}] = \sum_{i=1}^{4}\begin{bmatrix} N_i & 0 & 0 & 0 & 0 \\ 0 & N_i & 0 & 0 & 0 \\ 0 & 0 & N_i & 0 & 0 \\ 0 & 0 & 0 & N_i & 0 \\ 0 & 0 & 0 & 0 & N_i \end{bmatrix} \quad (21)$$

and **[IPV]** is the inertia matrix which is introduced as

$$[\boldsymbol{IPV}] = \sum_{i=1}^{4}\begin{bmatrix} I & 0 & 0 & P & 0 \\ 0 & I & 0 & 0 & P \\ 0 & 0 & I & 0 & 0 \\ P & 0 & 0 & V & 0 \\ 0 & P & 0 & 0 & V \end{bmatrix} \quad (22)$$

Free vibration analysis of such a flat laminated composite plate is performed by solving eigenvalue problems via the finite element method in which global stiffness and mass matrices. Similarly, the same equations and techniques are applied to perform free vibration analysis for a curved laminated composite plate. However, there is a difference for curved plates (Qatu 2002) in terms of strain components which is given as

$$\varepsilon_{xx} = \frac{\partial u}{\partial x} = \frac{\partial u_0}{\partial x} - \frac{w}{R_{xx}} - z\frac{\partial \theta_y}{\partial x}$$
$$\varepsilon_{yy} = \frac{\partial v}{\partial y} = \frac{\partial v_0}{\partial y} - \frac{w}{R_{yy}} + z\frac{\partial \theta_x}{\partial y}$$
$$\gamma_{xy} = \frac{\partial u}{\partial y} + \frac{\partial v}{\partial x} = \frac{\partial v_0}{\partial x} + \frac{\partial u_0}{\partial y} - \frac{2w}{R_{xy}} + z\left(\frac{\partial \theta_x}{\partial x} - \frac{\partial \theta_y}{\partial y}\right) \quad (23)$$
$$\gamma\varepsilon_{xz} = -\theta_y + \frac{\partial w}{\partial x}$$
$$\gamma_{yz} = \theta_x + \frac{\partial w}{\partial y}$$

Implementing Eq. (23) in the same way in laminated flat plates enables one to find element stiffness matrix and element mass matrix. Since the structure that is investigated in this study comprises singly curved plate, additional terms w/R_{yy} and $2w/R_{xy}$ are neglected. Thus, the $\mathbf{[B_s]}$ matrix becomes

$$[\boldsymbol{B_{sc}}] = \begin{bmatrix} \varepsilon_{xx} \\ \varepsilon_{yy} \\ \gamma_{xy} \\ \gamma_{xz} \\ \gamma_{yz} \end{bmatrix} = \sum_{i=1}^{4}\begin{bmatrix} \frac{\partial N_i}{\partial x} & 0 & -\frac{w}{R_{xx}} & 0 & 0 \\ 0 & \frac{\partial N_i}{\partial y} & -\frac{w}{R_{yy}} & 0 & 0 \\ \frac{\partial N_i}{\partial y} & \frac{\partial N_i}{\partial x} & 0 & 0 & 0 \\ 0 & 0 & 0 & 0 & -\frac{\partial N_i}{\partial x} \\ 0 & 0 & 0 & \frac{\partial N_i}{\partial y} & 0 \\ 0 & 0 & 0 & \frac{\partial N_i}{\partial x} & -\frac{\partial N_i}{\partial y} \\ 0 & 0 & \frac{\partial N_i}{\partial x} & 0 & -N_i \\ 0 & 0 & \frac{\partial N_i}{\partial y} & N_i & 0 \end{bmatrix}\begin{bmatrix} u_i \\ v_i \\ w_i \\ \theta_{xi} \\ \theta_{yi} \end{bmatrix} \quad (24)$$

Table 1 The first ten natural frequencies for fixed LCPTPF structure for different radii of curvature for P1

Freq. No	$R_{xx} = 500h$			$R_{xx} = 250h$			$R_{xx} = 100h$			$R_{xx} = 10h$		
	Ansys (Hz)	Present Work (Hz)	Err. %	Ansys (Hz)	Present Work (Hz)	Err. %	Ansys (Hz)	Present Work (Hz)	Err. %	Ansys (Hz)	Present Work (Hz)	Err. %
1	78.88	75.13	4.75	78.953	75.13	4.84	78.84	75.14	4.69	77.01	75.79	1.58
2	135.48	135.79	0.23	135.49	135.79	0.22	135.39	135.78	0.29	131.42	134.65	2.46
3	148.13	154.96	4.61	148.27	154.96	4.51	148.07	154.96	4.65	145.53	155.09	6.57
4	270.98	276.70	2.11	271.41	276.67	1.94	269.21	276.43	2.68	243.97	259.02	6.17
5	276.17	278.66	0.90	276.47	278.63	0.78	274.26	278.41	1.51	245.24	261.15	6.49
6	309.09	314.12	1.63	309.87	314.14	1.38	308.97	314.25	1.71	304.76	314.72	3.27
7	311.79	323.76	3.84	312.25	323.80	3.70	310.34	324.04	4.41	305.18	320.68	5.08
8	339.15	326.28	3.79	340.14	325.87	4.20	338.97	324.62	4.23	335.42	341.28	1.75
9	345.98	327.28	5.40	347.96	327.72	5.82	349.42	329.14	5.80	351.82	347.09	1.34
10	347.96	354.15	1.78	349.83	354.09	1.22	351.36	353.69	0.66	369.63	350.46	5.19

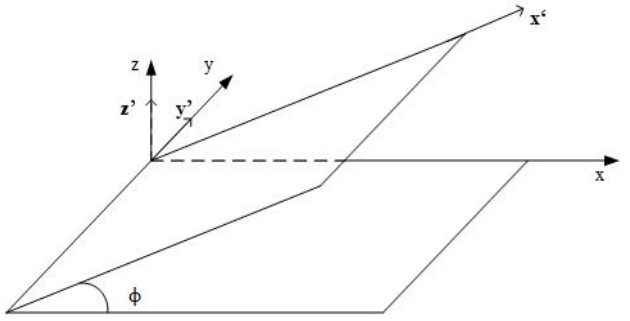

Fig. 5 Transformation of local coordinates

Replacing **[Bs]** to **[B_{sc}]** in Eq. (15) gives element stiffness matrix for a singly curved plate. The element mass matrix equation is the same as Eq. (20).

FSDT is an effective theory for free vibration analysis of laminated composite plates individually. Drilling effect is neglected in vibration analysis of laminated composite flat/curved plates when FSDT is used. However, in order to perform free vibration analysis of structures (i.e., frames), the addition of the drilling effect *(θ_z)* is necessary to satisfy all DOF. Therefore, it is needed to expand the dimensions of the element stiffness matrix and element mass matrix from 20x20 to 24x24. To perform such a process, the off-diagonal terms that correspond to the θ_z are taken as zero. On the other hand, the corresponding diagonal terms are considered a quite small positive number, which is 1000 times smaller than the smallest diagonal term of the corresponding element matrix.

Following the implementation of the drilling effect, displacement terms are rotated by using Eq. (25) in order to model the LCPTPF structure. The rotation process is completed by rotating the original plate 90 and 270 degrees around its y-axis, as it is shown in Fig. 5.

$$\{u'\} = [\boldsymbol{T}]\{u\} \tag{25}$$

where **[T]** is the transformation matrix. The transformation matrix is given in Appendix A. *{u'}* is the vector of the rotated displacement terms and *{u}* is the displacement vector of the original displacement terms.

After considering the transformation matrix for each node, the element stiffness and element mass matrix of rotated plate is derived from

$$[\boldsymbol{K_e}] = [\boldsymbol{T}]^T[\boldsymbol{k_e}][\boldsymbol{T}]$$
$$[\boldsymbol{M_e}] = [\boldsymbol{T}]^T[\boldsymbol{m_e}][\boldsymbol{T}] \tag{26}$$

The dynamic response of LCPTPF for a conservative system can be formulated by means of Lagrange's equation of motion in the matrix form as

$$\left([\boldsymbol{K_{global}}] - \omega^2[\boldsymbol{M_{global}}]\right)q = 0 \tag{27}$$

3. Numerical results

In this study free vibration analysis of the LCPTPF, as shown in Fig. 1, is investigated in terms of the effect of radii of curvature, aspect ratio, boundary conditions and multi – bay case. Stacking sequences are set as [$0^0/0^0/0^0/0^0$], [$0^0/90^0/90^0/0^0$], [$90^0/0^0/0^0/90^0$], [$0/45^0/-45^0/0^0$] and [$0^0/60^0/-60^0/0^0$] for all cases. These stacking sequences are denoted as P1, P2, P3, P4 and P5 in order to simplify. Material properties are given in Appendix A (Reddy 2003). Natural frequency values are obtained in hertz (Hz) for each case mentioned below.

3.1 The effect of radii of curvature

Four different radii of curvature parameter, which is depended on thickness *(h)*, is introduced. Radii of curvature *(R_{xx})* are ranged gradually from 500h to 10h. Other structure dimensions are set as a=ac=b=0.8 m, and b/h=10 and is fixed from both ends. Finite element analysis is performed with a mesh size of 30x30. For comparison of the accuracy, the same structure is also modeled using ANSYS. The natural frequencies obtained from analysis of the structure are given in Tables 1-5.

Table 2 The first ten natural frequencies for fixed LCPTPF structure for different radii of curvature for P2

Freq. No	$R_{xx} = 500h$			$R_{xx} = 250h$			$R_{xx} = 100h$			$R_{xx} = 10h$		
	Ansys (Hz)	Present Work (Hz)	Err. %	Ansys (Hz)	Present Work (Hz)	Err. %	Ansys (Hz)	Present Work (Hz)	Err. %	Ansys (Hz)	Present Work (Hz)	Err. %
1	74.42	70.87	4.76	74.60	70.87	4.99	74.37	70.88	4.69	72.61	71.28	1.83
2	131.75	132.18	0.33	131.83	132.17	0.26	131.62	132.16	0.41	127.30	130.96	2.88
3	143.88	152.83	6.22	144.30	152.83	5.91	143.81	152.83	6.27	141.09	152.95	8.41
4	254.75	260.30	2.18	256.52	260.26	1.46	253.17	259.99	2.69	230.05	239.24	3.99
5	260.28	264.12	1.48	261.70	264.08	0.91	258.60	263.83	2.02	232.47	244.23	5.06
6	299.10	307.29	2.74	301.17	307.32	2.04	298.95	307.55	2.88	294.90	304.52	3.26
7	326.39	311.04	4.70	330.00	310.98	5.76	329.47	310.62	5.72	333.41	323.32	3.03
8	328.66	316.26	3.77	331.94	316.35	4.70	331.75	316.88	4.48	353.20	334.13	5.40
9	343.05	364.31	6.20	346.26	364.31	5.21	342.62	364.31	6.33	364.38	364.53	0.04
10	370.33	379.79	2.55	373.08	379.83	1.81	369.67	380.17	2.84	377.75	394.53	4.44

Table 3 The first ten natural frequencies for fixed LCPTPF structure for different radii of curvature for P3

Freq.No	$R_{xx} = 500h$			$R_{xx} = 250h$			$R_{xx} = 100h$			$R_{xx} = 10h$		
	Ansys (Hz)	Present Work (Hz)	Err. %	Ansys (Hz)	Present Work (Hz)	Err. %	Ansys (Hz)	Present Work (Hz)	Err. %	Ansys (Hz)	Present Work (Hz)	Err. %
1	36.54	34.34	6.02	36.53	34.34	5.99	36.51	34.35	5.90	35.43	35.52	0.27
2	131.63	132.14	0.39	131.56	132.14	0.44	131.29	132.09	0.61	118.72	128.38	8.14
3	133.81	144.92	8.30	133.79	144.92	8.32	133.73	144.92	8.37	122.30	144.93	18.50
4	135.70	150.33	10.78	135.50	150.33	10.94	134.88	150.30	11.43	131.32	148.05	12.74
5	152.57	168.37	10.36	152.36	168.37	10.51	151.77	168.37	10.94	145.22	168.65	16.13
6	201.80	202.94	0.56	201.24	202.95	0.85	201.34	203.04	0.84	193.20	211.50	9.47
7	204.03	215.61	5.68	204.52	215.62	5.43	204.01	215.70	5.73	198.34	222.60	12.23
8	204.31	247.47	21.12	204.52	247.47	21.00	205.99	247.47	20.14	225.62	248.78	10.27
9	213.33	254.46	19.28	213.86	254.46	18.98	215.44	254.46	18.11	234.82	254.47	8.37
10	384.35	403.82	5.07	384.31	403.82	5.08	384.14	403.81	5.12	369.12	403.29	9.26

Table 1 shows the first ten natural frequencies for P1 in accordance with the change of radii of curvature. It has been seen from Table 1 that as R_{xx} decreases, low frequency values decrease while high frequency values increase.

The First ten natural frequency values of P2 are given in Table 2. The first six natural frequency values decrease when R_{xx} decreases. On the other hand, other natural frequency values increase as the radii of curvature decreases.

Table 3 presents the first ten natural frequency values of P3. Similarly, to the natural frequency results of P1, which is given in Table 1, low frequency values decrease as R_{xx} decreases.

On the other hand, high frequency values increase as R_{xx} decreases.

According to Tables 4 and 5, natural frequency values of P4 and P5 trend is the same as P2. Outcomes of the present study are in good agreement with ANSYS results. It is seen from the results given in this section, the first five natural frequencies of all structures, regardless of their stacking sequence, decrease as R_{xx} decreases. Other natural frequency values behave differently with respect to the stacking sequence. The last five natural frequency values increase for P2, P4, and P5 when R_{xx} decreases. The ninth and tenth natural frequency values of P1 increase as R_{xx} decreases. Other natural frequency values of P1 behaves in the opposite way. The eighth and ninth natural frequency values of P3 increases when R_{xx} decrease. Other natural frequency values of P3 decrease as R_{xx} decreases. Although there are some differences between ANSYS results, the present work shows in a good agreement with ANSYS results, especially when R_{xx} increases. This is because the representation ability of the selected finite element for the curved part of the structure is very good for slightly curved structures. The stacking sequence has also affected the increment and the values of natural frequencies.

In addition, it is concluded that the representation of the present study changes with respect to the fiber angle of each layer. Furthermore, it is observed that the fiber angle of the first and the last layer is more effective than those of the middle layer on the ability of representation of this study.

Table 4 The first ten natural frequencies for fixed LCPTPF structure for different radii of curvature for P4

Freq. No	$R_{xx}=500h$			$R_{xx}=250h$			$R_{xx}=100h$			$R_{xx}=10h$		
	Ansys (Hz)	Present Work (Hz)	Err. %	Ansys (Hz)	Present Work (Hz)	Ansys (Hz)	Present Work (Hz)	Err. %	Ansys (Hz)	Ansys (Hz)	Ansys (Hz)	Present Work (Hz)
1	74.67	71.60	4.10	74.86	71.60	4.35	74.62	71.61	4.03	72.85	72.10	1.02
2	255.59	264.13	3.34	257.37	264.10	2.61	254.02	263.84	3.87	218.02	241.90	10.95
3	258.09	273.47	5.96	258.60	273.38	5.72	255.29	272.80	6.86	230.76	244.28	5.86
4	271.88	281.83	3.66	273.00	281.78	3.22	271.42	281.51	3.72	263.86	279.81	6.04
5	294.71	289.15	1.89	295.45	289.24	2.10	294.88	289.79	1.73	290.22	297.70	2.58
6	305.31	312.68	2.41	306.64	312.71	1.98	306.22	312.94	2.19	328.07	328.95	0.27
7	327.18	321.10	1.86	330.80	321.12	2.93	330.30	321.30	2.72	333.86	341.06	2.16
8	332.93	328.91	1.21	336.14	329.12	2.09	336.18	330.55	1.67	343.56	359.85	4.74
9	343.43	371.03	8.04	346.62	371.04	7.05	343.06	371.04	8.16	363.61	371.47	2.16
10	354.23	375.7	6.06	356.91	375.75	5.28	355.41	376.13	5.83	365.61	384.74	5.23

Table 5 The first ten natural frequencies for fixed LCPTPF structure for different radii of curvature for P5

Freq. No	$R_{xx}=500h$			$R_{xx}=250h$			$R_{xx}=100h$			$R_{xx}=10h$		
	Ansys (Hz)	Present Work (Hz)	Err. %	Ansys (Hz)	Present Work (Hz)	Ansys (Hz)	Present Work (Hz)	Err. %	Ansys (Hz)	Ansys (Hz)	Ansys (Hz)	Present Work (Hz)
1	74.85	71.17	4.92	75.04	71.17	5.15	74.80	71.18	4.84	73.02	71.61	1.93
2	245.86	258.76	5.25	245.65	258.67	5.30	243.41	258.11	6.04	210.04	231.28	10.11
3	249.35	260.31	4.40	250.14	260.31	4.07	248.96	260.32	4.56	231.74	241.18	4.07
4	256.53	262.04	2.15	258.33	262.01	1.42	254.95	261.75	2.67	241.79	260.42	7.71
5	269.35	270.46	0.41	270.65	270.50	0.06	269.72	270.77	0.39	266.87	275.70	3.31
6	300.11	309.85	3.25	301.19	309.88	2.89	301.04	310.11	3.01	324.24	325.95	0.53
7	329.61	316.93	3.85	333.29	316.95	4.90	332.72	317.11	4.69	336.27	332.54	1.11
8	333.07	329.75	1.00	336.24	329.95	1.87	336.12	331.32	1.43	342.48	356.71	4.15
9	345.06	367.51	6.51	347.62	367.51	5.72	345.62	367.52	6.34	351.50	367.78	4.63
10	346.01	369.46	6.78	349.23	369.54	5.82	346.04	370.10	6.95	367.88	392.19	6.61

3.2 The effect of aspect ratio

The effect of aspect ratio on the dynamic response of LCPTPF is investigated in this section. Four different aspect ratio which only changes with respect to the structure height *(a)* is taken into account and the structure is fixed from two sides. Structure dimensions are set as a=0.8 m to 1.6 m with 0.4 m increment, ac=b=0.8 m, R_{xx}/h=10 and b/h=10. For comparison, the same structure is modeled via ANSYS. The natural frequency results for this case are given in Tables 6-10.

According to results given in Table 6, the natural frequency values of P1 change significantly with respect to aspect ratio. As aspect ratio rises, all natural frequencies declines.

As it is expected, the error values decrease when the aspect ratio has smaller values.

Table 7 shows the first ten natural frequency values of P2. It can be concluded that the interpretation of P1 can also be made for P2 since the natural frequency values of P2 are changing in the same way as P1's.

As can be seen from the results which are given in Table 8, the aspect ratio has the same effect on P3 as other structures,

The natural frequency values of P2 are greater due to the stacking sequence when compared with P1. Again, the same trend as P1 in terms of error rate can be seen for P2.

P1 and P2. The natural frequency values are smaller than P1's and diminishing with respect to declining in the aspect ratio. The error rates are relatively higher than those of P1 and P2.

The first ten natural frequency values of P4 and P5 are given in Tables 9-10. It is seen that the fundamental frequencies of P4 and P5 for all aspect ratios are almost equal. The aspect ratio has the same effect as the other structures with different stacking sequences. The natural frequency values of P4 and P5 decreases as the aspect ratio increases. The error rates of the present study decrease when the value of the aspect ratio also decreases. For all structures with different stacking sequences, it can be concluded from the results given in this section that the increment of the aspect ratio affects the natural frequency

Table 6 The first ten natural frequencies of fixed LCPTPF structure with different aspect ratios for P1

Freq. No	$\frac{a}{b}=0.5$			$\frac{a}{b}=1$			$\frac{a}{b}=1.5$			$\frac{a}{b}=2$		
	Ansys (Hz)	Present Work (Hz)	Err. %	Ansys (Hz)	Present Work (Hz)	Err. %	Ansys (Hz)	Present Work (Hz)	Err. %	Ansys (Hz)	Present Work (Hz)	Err. %
1	163.27	163.39	0.07	77.01	75.79	1.58	44.54	43.93	1.37	28.89	28.75	0.46
2	202.68	196.81	2.90	131.42	134.65	2.46	96.30	98.27	2.05	73.77	76.06	3.10
3	261.62	251.93	3.70	145.53	155.09	6.57	99.53	110.10	10.62	74.69	85.39	14.33
4	305.22	314.27	2.97	243.97	259.02	6.17	161.99	180.23	11.26	109.12	121.65	11.48
5	315.27	321.39	1.94	245.24	261.15	6.49	166.03	181.38	9.25	113.90	124.95	9.70
6	374.37	382.38	2.14	304.76	314.72	3.27	190.97	194.92	2.07	130.35	132.28	1.48
7	494.60	480.02	2.95	305.18	320.68	5.08	212.71	210.03	1.26	142.69	142.84	0.11
8	516.39	518.44	0.40	335.42	341.28	1.75	217.21	225.06	3.61	171.54	176.44	2.86
9	561.38	540.67	3.69	351.82	347.09	1.34	224.82	231.38	2.92	174.92	179.24	2.47
10	595.49	594.04	0.24	369.63	350.46	5.19	276.37	275.55	0.30	223.17	231.70	3.82

Table 7 The first ten natural frequencies of fixed LCPTPF structure with different aspect ratios for P2

Freq. No	$\frac{a}{b}=0.5$			$\frac{a}{b}=1$			$\frac{a}{b}=1.5$			$\frac{a}{b}=2$		
	Ansys (Hz)	Present Work (Hz)	Err. %	Ansys (Hz)	Present Work (Hz)	Err. %	Ansys (Hz)	Present Work (Hz)	Err. %	Ansys (Hz)	Present Work (Hz)	Err. %
1	154.70	154.32	0.25	72.61	71.28	1.83	41.89	41.22	1.60	27.13	26.96	0.61
2	193.35	199.10	2.97	127.30	130.96	2.88	91.55	93.91	2.59	68.92	71.20	3.32
3	246.65	256.71	4.08	141.09	152.95	8.41	94.88	108.88	14.76	69.50	85.01	22.33
4	296.40	282.98	4.53	230.05	239.24	3.99	152.81	169.34	10.82	102.81	114.63	11.50
5	306.10	297.97	2.66	232.47	244.23	5.06	157.27	171.86	9.28	107.93	118.65	9.93
6	460.76	456.86	0.85	294.90	304.52	3.26	182.51	186.19	2.02	124.29	126.39	1.69
7	482.07	496.09	2.91	333.41	323.32	3.03	201.05	198.16	1.44	134.54	134.60	0.04
8	599.91	627.32	4.57	353.20	334.13	5.40	262.65	260.10	0.97	211.14	220.57	4.47
9	601.96	648.52	7.73	364.38	364.53	0.04	284.68	274.40	3.61	222.52	233.92	5.12
10	608.08	656.85	8.02	377.75	394.53	4.44	295.93	306.83	3.68	230.94	237.98	3.05

Table 8 The first ten natural frequencies of fixed LCPTPF structure with different aspect ratios for P3

Freq. No	$\frac{a}{b}=0.5$			$\frac{a}{b}=1$			$\frac{a}{b}=1.5$			$\frac{a}{b}=2$		
	Ansys (Hz)	Present Work (Hz)	Err. %	Ansys (Hz)	Present Work (Hz)	Err. %	Ansys (Hz)	Present Work (Hz)	Err. %	Ansys (Hz)	Present Work (Hz)	Err. %
1	86.94	88.85	2.19	35.43	35.52	0.27	19.20	19.78	3.02	12.03	12.98	7.91
2	163.19	174.39	6.86	118.72	128.38	8.14	75.45	93.22	23.55	48.17	64.74	34.40
3	174.77	189.76	8.58	122.30	144.93	18.50	85.29	97.90	14.79	59.38	69.43	16.93
4	225.79	228.08	1.01	131.32	148.05	12.74	86.01	99.01	15.12	61.46	71.23	15.90
5	226.46	250.28	10.52	145.22	168.65	16.13	94.83	113.72	19.92	66.37	73.43	10.64
6	374.57	467.65	24.85	193.20	211.50	9.47	105.85	113.91	7.61	69.73	77.27	10.82
7	388.56	472.17	21.52	198.34	222.60	12.23	118.65	127.96	7.85	83.15	93.89	12.92
8	459.97	504.85	9.76	225.62	248.78	10.27	160.11	180.89	12.98	119.81	150.60	25.70
9	494.71	578.41	16.92	234.82	254.47	8.37	171.22	192.44	12.39	135.04	166.59	23.36
10	502.96	600.43	19.38	369.12	403.29	9.26	241.93	279.05	15.34	156.73	186.78	19.17

Table 9 The first ten natural frequencies of fixed LCPTPF structure with different aspect ratios for P4

Freq. No	$\frac{a}{b}=0.5$			$\frac{a}{b}=1$			$\frac{a}{b}=1.5$			$\frac{a}{b}=2$		
	Ansys (Hz)	Present Work (Hz)	Err. %	Ansys (Hz)	Present Work (Hz)	Err. %	Ansys (Hz)	Present Work (Hz)	Err. %	Ansys (Hz)	Present Work (Hz)	Err. %
1	155.09	156.75	1.07	72.85	72.10	1.02	42.05	41.61	1.02	27.24	27.20	0.14
2	278.78	282.44	1.31	218.02	241.90	10.95	153.26	166.14	8.40	100.88	112.25	11.27
3	297.35	289.40	2.67	230.76	244.28	5.86	154.09	172.05	11.66	103.14	116.19	12.65
4	516.80	514.18	0.51	263.86	279.81	6.04	154.29	174.28	12.96	109.18	119.92	9.84
5	529.04	562.27	6.28	290.22	297.70	2.58	174.81	182.49	4.39	117.28	125.00	6.58
6	552.15	579.23	4.90	328.07	328.95	0.27	201.52	201.01	0.25	134.92	136.26	0.99
7	601.54	664.27	10.43	333.86	341.06	2.16	211.82	214.08	1.07	146.68	150.58	2.66
8	609.99	675.02	10.66	343.56	359.85	4.74	234.26	255.46	9.05	186.10	205.29	10.31

Table 10 The first ten natural frequencies of fixed LCPTPF structure with different aspect ratios for P5

Freq. No	$\frac{a}{b}=0.5$			$\frac{a}{b}=1$			$\frac{a}{b}=1.5$			$\frac{a}{b}=2$		
	Ansys (Hz)	Present Work (Hz)	Err. %	Ansys (Hz)	Present Work (Hz)	Err. %	Ansys (Hz)	Present Work (Hz)	Err. %	Ansys (Hz)	Present Work (Hz)	Err. %
1	156.02	155.41	0.39	73.01	71.61	1.92	42.06	41.36	1.65	27.20	27.04	0.56
2	275.69	276.03	0.12	210.04	231.28	10.11	144.13	157.79	9.48	95.35	108.19	13.47
3	299.04	285.57	4.50	231.72	241.18	4.08	146.46	159.19	8.69	103.28	110.39	6.88
4	465.57	492.50	5.78	241.79	260.42	7.71	153.70	170.50	10.93	103.73	115.31	11.16
5	471.47	516.02	9.45	266.87	275.70	3.31	164.79	178.59	8.37	111.40	122.70	10.14
6	513.22	539.00	5.02	324.24	325.95	0.53	202.48	199.40	1.52	135.31	135.29	0.01
7	605.83	655.00	8.12	336.27	332.54	1.11	203.44	205.44	0.98	140.06	144.22	2.97
8	610.40	661.13	8.31	342.48	356.71	4.15	233.86	266.05	13.76	186.94	222.69	19.12
9	647.09	701.92	8.47	351.50	367.78	4.63	237.07	276.6	16.67	187.68	226.61	20.74
10	661.34	713.22	7.84	367.88	392.19	6.61	286.95	279.00	2.77	232.47	239.81	3.16

Table 11 The first ten natural frequencies of P1 with fixed and simply supported boundary conditions

Freq. No	SS			CC		
	Ansys (Hz)	Present Work (Hz)	Err. %	Ansys (Hz)	Present Work (Hz)	Err. %
1	39.76	37.13	6.59	77.01	75.797	1.58
2	131.26	134.61	2.55	131.42	134.65	2.46
3	135.38	145.79	7.69	145.53	155.09	6.57
4	213.65	235.46	10.21	243.97	259.02	6.17
5	218.47	238.83	9.32	245.24	261.15	6.49
6	272.26	279.81	2.77	304.76	314.72	3.27
7	277.37	291.74	5.18	305.18	320.68	5.08
8	298.51	302.17	1.23	335.42	341.28	1.75
9	312.94	309.42	1.12	351.82	347.09	1.34
10	349.86	326.99	6.54	369.63	350.46	5.19

values. As the aspect ratio increases, the natural frequency values of those structures decrease. This is because when the aspect ratio increase, the stiffness matrix of the structure decrease.

3.3 The effect of boundary conditions

In this section, LCPTPF structure with two sides fixed

Table 12 The first ten natural frequencies of P2 with fixed and simply supported boundary conditions

Freq. No	SS			CC		
	Ansys (Hz)	Present Work (Hz)	Err. %	Ansys (Hz)	Present Work (Hz)	Err. %
1	37.36	34.61	7.34	72.61	71.28	1.83
2	127.11	130.93	3.01	127.30	130.96	2.88
3	131.25	144.33	9.97	141.09	152.95	8.41
4	201.14	218.18	8.47	230.05	239.24	3.99
5	206.81	223.99	8.31	232.47	244.23	5.06
6	261.86	268.96	2.71	294.90	304.52	3.26
7	295.55	284.62	3.70	333.41	323.32	3.03
8	332.40	310.35	6.63	353.20	334.13	5.40
9	341.96	335.57	1.87	364.38	364.53	0.04
10	353.17	368.75	4.41	377.75	394.53	4.44

Table 13 The first ten natural frequencies of P3 with fixed and simply supported boundary conditions

Freq. No	SS			CC		
	Ansys (Hz)	Present Work (Hz)	Err. %	Ansys (Hz)	Present Work (Hz)	Err. %
1	16.95	15.76	7.02	35.43	35.52	0.27
2	97.45	124.87	28.14	118.72	128.38	8.14
3	109.26	125.69	15.04	122.3	144.93	18.50
4	119.79	132.88	10.93	131.32	148.05	12.74
5	133.18	151.36	13.65	145.22	168.65	16.13
6	153.90	159.56	3.68	193.20	211.50	9.47
7	171.13	179.20	4.72	198.34	222.60	12.23
8	199.93	217.37	8.72	225.62	248.78	10.27
9	212.36	223.37	5.18	234.82	254.47	8.37
10	357.55	389.04	8.81	369.12	403.29	9.26

Table 14 The first ten natural frequencies of P4 with fixed and simply supported boundary conditions

Freq. No	SS			CC		
	Ansys (Hz)	Present Work (Hz)	Err. %	Ansys (Hz)	Present Work (Hz)	Err. %
1	37.50	34.93	6.85	72.85	72.10	1.02
2	199.68	221.89	11.12	218.02	241.9	10.95
3	201.64	228.14	13.14	230.76	244.28	5.86
4	230.39	250.09	8.55	263.86	279.81	6.04
5	265.63	277.11	4.32	290.22	297.70	2.58
6	291.81	288.71	1.06	328.07	328.95	0.27
7	295.69	312.08	5.54	333.86	341.06	2.16
8	310.49	328.34	5.75	343.56	359.85	4.74
9	341.68	341.55	0.04	363.61	371.47	2.16
10	347.76	361.83	4.05	365.61	384.74	5.23

Table 15 The first ten natural frequencies of P5 with fixed and simply supported boundary conditions

Freq. No	SS			CC		
	Ansys (Hz)	Present Work (Hz)	Err. %	Ansys (Hz)	Present Work (Hz)	Err. %
1	37.50	34.71	7.44	73.02	71.61	1.93
2	194.55	219.49	12.82	210.04	231.28	10.11
3	202.14	220.88	9.27	231.74	241.18	4.07
4	213.73	235.12	10.01	241.79	260.42	7.71
5	241.53	257.19	6.48	266.87	275.70	3.31
6	284.97	286.31	0.47	324.24	325.95	0.53
7	297.23	299.78	0.86	336.27	332.54	1.11
8	306.49	327.81	6.96	342.48	356.71	4.15
9	326.22	338.24	3.68	351.50	367.78	4.63
10	344.97	367.22	6.45	367.88	392.19	6.61

Table 16 Mode shapes of fixed from two ends LCPTPF

Mode	*P1*	*P2*	*P3*	*P4*	*P5*
1	Bn/Ln	Bn/Ln	Bn/Ln	Bn/Ln	Bn/Ln
2	Bn/Ln	Bn/Ln	Tr/Bn	Tr/Bn	Tr/Bn
3	Tr/Bn	Tr/Bn	Bn	Bn	Bn
4	Bn	Bn	Tr/Bn	Tr/Bn	Tr/Bn
5	Tr/Bn	Tr/Bn	Tr/Bn	Tr/Bn	Tr/Bn
6	Bn	Tr	Bn	Bn	Bn
7	Tr	Bn	Tr	Bn	Bn
8	Bn	Tr/Bn	Bn	Bn	Bn
9	Bn	Bn	Tr/Bn	Bn	Bn
10	Tr/Bn	Bn	Bn	Bn	Bn

*Bn: Bending; *Ln:Longitudinal; *Tr:Torsion

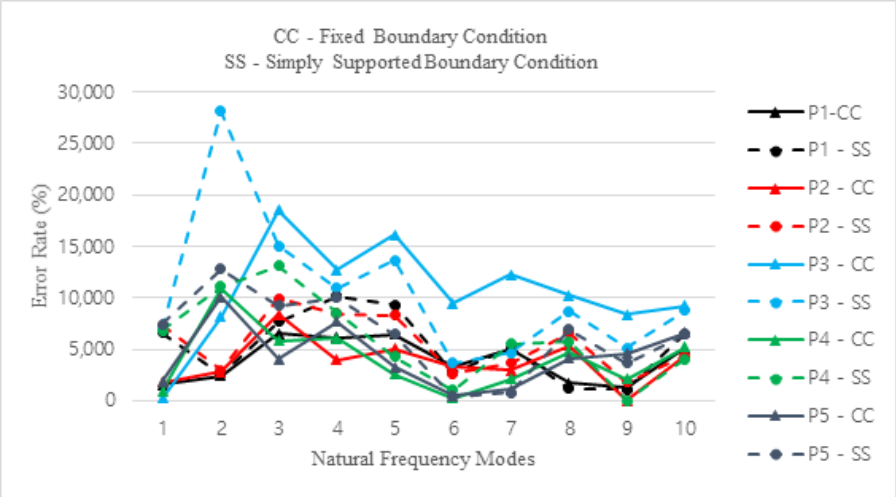

Fig. 6 The error rates of LCPTPF with all stacking orders for fixed and simply supported boundary conditions.

Table 17 Mode shapes of simply supported LCPTPF

Mode	*P1*	*P2*	*P3*	*P4*	*P5*
1	Bn/Ln	Bn/Ln	Bn/Ln	Bn/Ln	Bn/Ln
2	Bn/Ln	Bn/Ln	Bn	Tr/Bn	Tr/Bn
3	Tr	Tr	Tr/Bn	Bn	Bn
4	Bn	Bn	Tr/Bn	Tr/Bn	Tr/Bn
5	Tr/Bn	Tr/Bn	Tr/Bn	Tr/Bn	Tr/Bn
6	Bn	Bn	Bn	Bn	Bn
7	Bn	Bn	Tr/Bn	Bn	Bn
8	Bn	Tr/Bn	Bn	Bn	Bn
9	Bn	Bn	Tr/Bn	Bn	Bn
10	Tr/Bn	Bn	Bn	Bn	Bn

*Bn: Bending; *Ln:Longitudinal; *Tr:Torsion

(CC) and simply supported (SS) boundary conditions are investigated for P1, P2, P3, P4, and P5 stacking sequences. Structure dimensions are set as a=ac=b=0.8 m, $R_{xx}/h=10$ and b/h=10.

All mode shapes have been defined according to general deflection tendencies to form (i.e., Bn: Bending; Ln: Longitudinal; Tr: Torsion).

Tables 11 and 12 show the first ten natural frequency values of P1 and P2 for simply supported and fixed from two ends boundary conditions. It is seen that natural frequency values are greater for that of fixed boundary conditions.

Free vibration analysis results for P3 are given in Table 13. The natural frequency values are higher for that of fixed boundary conditions. A similar interpretation can be made for this stacking sequence. The error rates of the present study are relatively higher than those of P1 and P2.

The first ten natural frequency values for simply supported and two sides fixed boundary conditions for P4 and P5 are given in Tables 14-15, respectively.

As seen from Tables 14-15, changes in natural frequency for P5 and P4 are similar to P1, P2, and P3. Error rates change with respect to the mode of the structure for relevant boundary conditions, as seen in Fig. 6. Mode shapes for both boundary conditions are given in Tables 16 and 17.

For fixed from two sides boundary conditions, it can be seen from Table 16 that for all stacking orders, the first mode is the coupling of bending and longitudinal vibration. Two different vibration mode is observed for the second mode. P1 and P2 have the same vibration mode, which is the coupling of bending and longitudinal vibration. On the other hand, P3, P4, and P5 vibrate in torsional and bending coupled mode. For the third mode, while P1 and P2 vibrate in the torsional vibration mode, P3, P4, and P5 vibrate in the bending mode. The fourth mode is the symmetry of the third mode. P1 and P2 vibrate in the bending mode, whereas P3, P4, and P5 vibrate in the torsional mode. For the fifth mode, P1, P2, P3, P4, and P5 vibrate in the coupling of bending and torsional modes.

The sixth and the seventh and the eighth mode are the same for P1 and P3, which is the bending, torsional, and bending vibration, respectively. P2 behaves differently from all other stacking sequences after the fifth mode. P4 and P5 behave the same for all modes. This is because even they have different fiber angles, they have the same angle pattern.

It is seen from Table 17 that for simply supported boundary conditions, the same mode of the fixed boundary condition is present for all stacking sequences. For the second mode, there are three different vibration modes. P1 and P2 vibrate in the coupling of bending and longitudinal mode, whereas P4 and P5 vibrate in the coupling of torsion and bending mode. P3 is in the pure bending vibration in this mode. For the third mode, P1 and P2 are in the torsional vibration mode. P4 and P5 are in the bending mode. P3 vibrates in the coupling of torsional and bending mode. The fourth and the fifth modes have the same behaviour as of the fixed boundary condition for all stacking orders.

Different bending modes occur at the sixth modes for each stacking sequence. Except for P4 and P5, all stacking orders have different mode shapes for the seventh, eighth, ninth, and tenth modes.

It is concluded that no matter which boundary condition is applied, the first mode is the coupling of bending and longitudinal vibration regardless of the stacking order. For the other modes, the angle and the angle pattern change the vibration mode of the structure. In addition, except for the first and the sixth modes, the boundary condition also changes the mode of the structure as expected.

3.3 Multi-bay structure

Multi-Bay structure of LCPTPF, which is shown in Fig. 7, is investigated by using FSDT. The clamped boundary condition is selected for free vibration analysis. The natural frequency results are given in Tables 18-22.

Free vibration analysis results of multi-bay structure with P1 and P2 stacking orders are given in Tables 18-19, respectively. It is seen that the natural frequency values of the multi-bay structure for P1 and P2 are greater than the natural frequency values of P1 and P2 with single-bay (see Table 1 and Table 2). For the most modes, the present study is in good agreement with ANSYS results.

Table 18 The first ten natural frequencies of multi – bay P1 with fixed boundary conditions

Freq. No	Ansys (Hz)	Present Work (Hz)	Err. %
1	71.53	73.34	2.54
2	118.49	122.88	3.70
3	138.64	145.76	5.14
4	221.64	239.08	7.87
5	240.55	263.72	9.63
6	241.46	276.89	14.67
7	247.44	298.93	20.81
8	299.93	316.50	5.52
9	302.96	328.01	8.27
10	312.52	335.09	7.22

Table 19 The first ten natural frequencies of multi – bay P2 with fixed boundary conditions

Freq. No	Ansys (Hz)	Present Work (Hz)	Err. %
1	67.49	69.10	2.40
2	114.59	119.77	4.52
3	134.38	142.49	6.04
4	212.19	224.42	5.76
5	227.26	237.85	4.66
6	228.57	255.96	11.98
7	233.58	266.27	14.00
8	291.16	305.96	5.08
9	292.53	313.62	7.21
10	335.24	322.91	3.68

Table 20 The first ten natural frequencies of multi – bay P3 with fixed conditions

Freq. No	Ansys (Hz)	Present Work (Hz)	Err. %
1	32.96	37.90	15.01
2	108.95	118.60	8.86
3	122.93	139.01	13.08
4	124.46	168.06	35.03
5	129.38	181.46	40.25
6	140.6	191.93	36.51
7	149.43	198.02	32.52
8	196.83	228.18	15.93
9	197.34	233.71	18.43
10	219.84	242.45	10.28

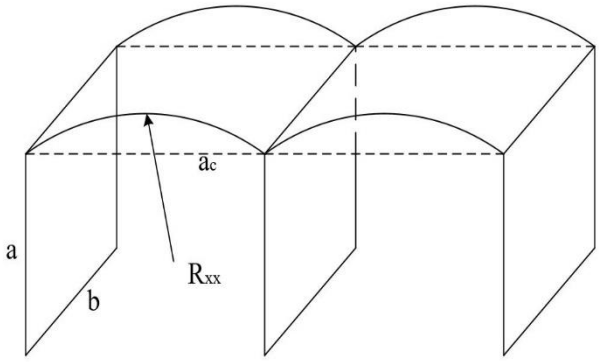

Fig. 7 Multi-Bay Structure of LCPTPF

Table 21 The first ten natural frequencies of multi – bay P4 with fixed boundary conditions

Freq. No	Ansys (Hz)	Present Work (Hz)	Err. %
1	67.71	70.03	3.43
2	208.56	244.37	17.17
3	226.66	251.32	10.88
4	228.05	274.68	20.45
5	234.26	276.39	17.98
6	276.91	292.05	5.47
7	283.62	298.14	5.12
8	328.11	328.79	0.21
9	335.49	337.81	0.69
10	337.6	350.17	3.72

Table 22 The first ten natural frequencies of multi – bay P5 with fixed boundary conditions

Freq. No	Ansys (Hz)	Present Work (Hz)	Err. %
1	67.87	69.49	2.40
2	193.52	229.42	18.55
3	220.49	240.19	8.93
4	229.19	257.51	12.36
5	235.24	269.14	14.41
6	256.43	276.86	7.97
7	265.39	283.38	6.78
8	323.34	325.66	0.72
9	334.73	333.13	0.48
10	338.39	340.80	0.71

Table 20 shows the first ten natural frequency values of fixed multi-bay structure with P3 stacking sequence. A similar interpretation of the natural frequency results of the multi-bay structure with P1 and P2 stacking sequence can also be made for this structure.

Tables 21 and 22 give the first ten natural frequency results for fixed multi-bay P4 and P5, respectively. Comparative results show that outcomes of the free vibration analysis of multi-bay structure with P4 and P5 stacking orders are similar to P1, P2, and P3.

4. Conclusions

In this study, finite element free vibration analysis of LCPTPF structure is investigated by using FSDT for various stacking orders. Parameters such as radii of curvature, aspect ratio, boundary conditions are taken into account in order to find out the ability of the representation of the present study. Additionally, free vibration analysis is also performed for the multi-bay structure of LCPTPF. Based on these analyses results, the following conclusions can be drawn as:

• It is concluded that the natural frequency values of such a structure depend on not only the stacking sequence but also the radii of curvature, aspect ratio, and boundary conditions. However, the stacking order and the aspect ratio have the most impact on the natural frequency values for the LCPTPF structure.

• In terms of stacking order, for all cases, fiber angles of the first and the last layer effects on the natural frequency values significantly.

• The radius of curvature has a slight effect on the natural frequency values of LCPTPF structure

• Regardless of stacking order, for all LCPTPF structures, the natural frequency values decrease considerably as the aspect ratio increases.

• The natural frequency values decrease as the boundary condition of the structure is set as simply supported. It is also concluded that the boundary condition is affected all structures similar regardless of their stacking sequence.

• According to results for multi-bay structure, the natural frequency values are higher when compared with single-bay structures.

• Except for P3, in general, the present study is in good agreement with ANSYS results. This is because the first and the last layer of the laminated composite structure affects the shear characteristics of the structure. Considering the representation of FSDT depends strongly on the shear correction factor, the natural frequency results of the present study for LCPTPF with P3 stacking order shows a moderate agreement with ANSYS results as it is expected. Nevertheless, the use of FSDT for free vibration analysis of the LCPTPF structure gives accurate results.

• The error rates decrease when Rxx increases.

• The error rates decrease when the aspect ratio gets higher values.

• According to the free vibration analysis results, the error rates change with respect to boundary conditions because mode shapes are different for each boundary condition and stacking order

• For multi-bay LCPTPF structures, the natural frequency results indicate that this study is in good agreement with ANSYS results for most natural frequency values. The error rates are relatively high when compared with the natural frequency results of one – bay LCPTPF structures.

• Although the error rates increase for some natural frequency values, the present study is in good agreement with ANSYS results for most natural frequency values.

• Mode shapes of this structure are depended on not only boundary conditions, but also the stacking order. In addition, the angle pattern affects the vibration mode considerably.

• Considering the mean errors of natural frequency results of LCPTPF, it is concluded that the combination of 4-node quadrilateral element and 4-node cylindrical shell element represents this structure in general.

• It can be concluded that using the novel approach, which is the combination of 4 – node quadrilateral element and 4 – node cylindrical shell element, for modeling LCPTPF in order to perform free vibration analysis of LCPTPF structure using finite element analysis is effective.

• The mathematical model of laminated composite parabolic thick plate frames, which is essential for future analyses (i.e., dynamic stability analysis) that could not be performed via computer-aided design programs such as ANSYS, is evaluated.

References

Afshari, P. and Widera, G.E.O. (2000), "Free vibration analysis of composite plates", *J. Pressure Vessel Technol.*, **122**, 390-398. doi:10.1115/1.556198

Atlihan, G., Çallıoglu, H., Conkur, E.S. and Topcu, M. (2009), "Free vibration analysis of laminated composite beams by using DQM", *J. Reinforced Plast. Compos.*, **28**, 881-892. https://doi.org/10.1177/0731684407087561

Belarbi, M.O., Tati, A., Houdayfa, O. and Khechai, A. (2017), "On the free vibration analysis of laminated composite and sandwich plates: a layerwise finite element formulation", Latin American *J. Solids Struct.*, **14**, 2265-2290. http://dx.doi.org/10.1590/1679-78253222

Cantin, G. and Clough, R.W. (1968), "A curved, cylindrical-shell, finite element", *AIAA J.*, **6**(6), 1057-1062. https://doi.org/10.2514/3.4673

Chakravorty, D., Bandyopadhyay, J.N. and Sinha, P.K. (1996), "Finite element free vibration analysis of doubly curved laminated composite shells", *J. Sound Vib.*, **191**(4), 491-504. https://doi.org/10.1006/jsvi.1996.0136

Chaubey, A.K. and Kumar, A. (2017), "Vibration of laminated composite shells with cutouts and concentrated mass", *Int. J. Res. Eng. Technol.*, **2**(9), 51-58. https://doi.org/10.2514/1.J056320

Civalek, O. (2017), "Vibration of laminated composite panels and curved plates with different types of FGM composite constituent", *Compos. Part B*, **122**, 89-108. https://doi.org/10.1016/j.compositesb.2017.04.012

El-Helloty, A. (2016), "Free vibration analysis of stiffened laminated composite plates", *Int. J. Comput. Appl.*, **156**(1), 12-23. DOI: 10.9790/1684-140301108123

Fallahi, N. and Delzendeh, M. (2018), "Free vibration analysis of laminated composite plates using meshless finite volume method", *Eng. Anal. with Bound. Elements*, **88**, 132-144. https://doi.org/10.1016/j.enganabound.2017.12.011

Ganesh, S., Keshava, S.K. and Mahato, P.K. (2016), "Free vibration analysis of delaminated laminated composite plates using finite element method", *Procedia Eng.*, **144**, 1067-1075.

https://doi.org/10.1016/j.proeng.2016.05.061
Hafizah, A.K.N., Viswanathan, K.K., Aziz, Z.A. and Lee, J.H. (2018), "Vibration of antisymmetric angle-ply composite annular plates of variable thickness", Journal of Mechanical Science and Technology, **32**(5), 2155-2162. doi: 10.1007/s12206-018-0424-1
Haldar, S. and Sheikh, A.H. (2005), "Free vibration analysis of isotropic and composite folded plates using a shear flexible element", *Finite Elem. Anal. Des.*, **42**, 208-226. https://doi.org/10.1016/j.finel.2005.06.003
Javed, S., Viswanathan, K.K. and Aziz, Z.A. (2016), "Free vibration analysis of composite cylindrical shells with non-uniform thickness walls", *Steel Compos. Struct.*, **20**(5), 1087-1102. http://dx.doi.org/10.12989/scs.2016.20.5.1087
Javed, S., Viswanathan, K., Aziz, Z., Karthik, K. and Lee, J. (2016), "Vibration of antisymmetric angle-ply laminated plates under higher order shear theory", *Steel Compos. Struct.*, **22**(6), 1281-1299. http://dx.doi.org/10.12989/scs.2016.22.6.1281
Javed, S., Viswanathan, K.K., Nurul Izyan, M.D., Aziz, Z.A. and Lee, J.H. (2018), "Free vibration of cross-ply laminated plates based on higher-order shear deformation theory", *Steel Compos. Struct.*, **26**, 473-484. https://doi.org/10.12989/scs.2018.26.4.473
Jun, L. and Hongxing, H. (1996), "Free vibration analyses of axially loaded laminated composite beams based on higher-order shear deformation theory", *Meccanica*, **46**, 1299-1317. https://doi.org/10.1007/s11012-010-9388-7
Liu, W.H., Huang, C.C. (1992), "Vibration analysis of folded plates", *J. Sound Vib.*, **157**(1), 123-137. https://doi.org/10.1016/0022-460X(92)90570-N
Marbur, S.R. and Kant, T. (1996), "Free vibration analysis of fiber reinforced composite beams using higher order theories and finite element modelling", *J. Sound Vib.*, **194**(3), 337-351. https://doi.org/10.1006/jsvi.1996.0362
Narita, Y. and Leissa, A.W. (1992), "Frequencies and mode shapes of cantilevered laminated composite plates", *J. Sound Vib.*, **154**(1), 161-172. https://doi.org/10.1016/0022-460X(92)90410-Y
Ngo-Cong, D., Mai-Duy, N., Karunasena, W. and Tran-Cong, T. (2011), "Free vibration analysis of laminated composite plates based on FSDT using one-dimensional IRBFN method", *Comput. Struct.*, **89**, 1-13. https://doi.org/10.1016/j.compstruc.2010.07.012
Niyogi, A.G., Laha, M.K. and Sinha, P.K. (1999), "Finite element vibration analysis of laminated composite folded plate structures", *Shock Vib.*, **6**, 273-283. http://dx.doi.org/10.1155/1999/354234
Ozturk, H. (2012), "Vibration analysis of a pre-stressed laminated composite curved beam", *Steel Compos. Struct.*, **19**(3), 635-659. https://doi.org/10.12989/scs.2015.19.3.635
Pandit, M. K., Haldar, S. and Mukhopadhyay, M. (2007), "Free vibration analysis of laminated composite rectangular plate using finite element method", *J. Reinf. Plast. Comp.*, **26**(1), 69-80. https://doi.org/10.1177/0731684407069955
Peng, L.X. (2015), "Free vibration analysis of symmetrically laminated folded plate structures using an element-free galerkin method", *Math.. Problem. Eng.*, 2015,13 pages. http://dx.doi.org/10.1155/2015/124296
Petyt, M. and Nath, J.M.D. (1971), "Vibration analysis of singly curved rectangular plates", *J. Sound Vib.*, **13**(4), 485-497. https://doi.org/10.1016/S0022-460X(70)80053-0
Qatu, M.S. (2002), "Recent research advances in the dynamic behavior of shells: 1989-200, Part 1: Laminated composite shells", *ASME Appl. Mech. Rev.*, **55**(4), 325-350. doi:10.1115/1.1483079
Ramtekkar, G.S. (2009), "Free vibration analysis of delaminated beams using mixed finite element method", *J. Sound Vib.*, **328**, 428-440. https://doi.org/10.1016/j.jsv.2009.08.008
Reddy, J.N. (2003), "*Mechanics of Laminated Composite Plates and Shells: Theory and Analysis, Second Edition*", CRC Press., U.S.A.
Thinh, T.I., Binh, B.V. and Tu, T.M. (2012), "Bending and vibration analysis of multi-folding laminate composite plate using finite element method", *Vietnam J. Mech.*, **34**(3), 185-202. http://dx.doi.org/10.15625/0866-7136/34/3/2359
Wittrick, W. and Horsington, R. (1984), "Buckling and vibration of composite folded-plate structures of finite length in combined shear and compression", *Proceedings of the Royal Society of London. Series A, Mathematical and Physical Sciences*, **392**(1802), 107-144. https://doi.org/10.1098/rspa.1984.0026
Yas, M.H. and Garmsiri, K. (2010), "Three-dimensional free vibration analysis of cylindrical shells with condinuous grading reinfrocement", *Steel Compos. Struct.*, **10**(4), 349-360. http://dx.doi.org/10.12989/scs.2010.10.4.349
Ye, T., Jin, G., Chen, Y., Ma, X. and Su, Z. (2013), "Free vibration analysis of laminated composite shallow shells with general elastic boundaries", *Compos. Struct.*, **106**, 470-490. https://doi.org/10.1016/j.compstruct.2013.07.005

CC

Nomenclature

a	The length of flat plates
a_c	The length of curved plate
b	The width of both flat plates and curved plate
E_1	Modulus of elasticity in x-direction
E_2	Modulus of elasticity in y-direction
G_{12}	Shear modulus with respect to x- and y- direction
G_{13}	Shear modulus with respect to x- and z- direction
G_{23}	Shear modulus with respect to y- and z- direction
h	The thickness of the structure
k	Number of lamina
N_i	Shape function of ith node of relevant finite element
p*	Shear correction factor
Q_{ij}	Stiffness components in global coordinates
q_{ij}	Stiffness components in local coordinates
R_{xx},R_{yy},R_{xy}	Radii of curvatures of curved plate
u,v,w	Displacement components with respect to x-, y- and z- axis of the plates
x,y,z	Global coordinates
x',y',z'	Rotated coordinates
z	Parametric thickness
[A]	Longitudinal stiffness matrix
[A_s]	Shear stiffness matrix
[B]	Longitudinal-bending coupled stiffness matrix
[Bs]	Strain matrix of flat plate
[B_{sc}]	Strain matrix of curved plate
[C]	Bending stiffness matrix
[D]	Stiffness matrix
[IPV]	Matrix of inertias
[k_e]	Element elastic stiffness matrix for un-rotated plates
[K_e]	Element elastic stiffness matrix for rotated plates
[K_{global}]	Global elastic stiffness matrix
[m_e]	Element mass matrix for un-rotated plates
[M_e]	Element mass matrix for rotated plates
[M_{global}]	Global mass matrix
[N]	Shape function matrix
$[Q_{bm}]$	Membrane-bending stiffness component matrix of global stiffness matrix
$[Q_s]$	Shear stiffness component matrix of global stiffness matrix
[T]	Transformation matrix
{u}	Displacement vector
{u'}	Rotated displacement vector
θ	Fiber angle
θ_x, θ_y	Rotations with respect to x- and y- axis
φ	Rotation angle
ν_{ij}	Strain in the i- direction because of the unit strain in j- direction (i=x,y ; j=x,y)
ρ	Density
σ_1, σ_2	Local stress components
σ_{xx}, σ_{yy}	Global stress components
τ_{12}, τ_{13}, τ_{23}	Local shear components
τ_{xy}, τ_{xz}, τ_{yz}	Global shear components
ω	Natural frequency